12th International Conference on Fracture Mechanics of Concrete and Concrete Structures
FraMCoS-12
B.L.A. Pichler, Ch. Hellmich, P. Preinstorfer (Eds)

https://doi.org/10.21012/FC12.1265
MS03-1:3

ROLE OF AGGREGATE PACKING IN ENHANCING CONCRETE FRACTURE RESPONSE: INSIGHTS FROM IN-SITU HIGH-SPEED IMAGING

N. KANEL[*], B. BATEN[*] AND N. GARG[*]

[*] University of Illinois Urbana Champaign
205 N Mathews Ave, Urbana, IL, United States of America
e-mail: nishantg@illinois.edu, cee.illinois.edu

Key words: Particle packing, High speed Digital Image Correlation (DIC), Fracture Process Zone (FPZ), Two Parameter Fracture Model (TPFM)

Abstract: Much of the existing literature has focused on improving concrete's fracture response by focusing on binder composition. However, the critical role of aggregates and their packing efficiency on fracture response has not been studied in detail. Here, we investigate the impact of packing enhancement on fracture behavior by designing 4 unique concrete mixes with customized aggregate skeletons, utilizing a continuous packing model. Fracture assessment using the two-parameter fracture model (TPFM) and high-speed cross-sectional Digital Image Correlation (DIC) was employed to acutely capture strain distribution and crack propagation from 95% of the pre-peak to the peak load. We find that improving coarse aggregate packing efficiency from 88% to 93%, while maintaining constant binder content, increased fracture energy (G_f) by 35.29% and 39.48% for 3 and 7 days respectively. Likewise, for 3 and 7 days the critical stress intensity factor (K_{1C}) increased by 46.08% and 51.66% respectively with the increase in packing efficiency. In summary, the results obtained quantify the impact of aggregate packing on concrete's fracture response.

1 INTRODUCTION

The quasi-brittle and heterogeneous nature of concrete results in a complex fracture process, including softening and hardening regime in the stress-strain curve [1], [2]. During the hardening phase of the stress-strain response, there is an onset of micro-cracks which is followed by a formation of macro-cracks in the softening regime [3], [4]. Due to this complexity of branching, coalescence, tortuosity and interlocking of the cracks, a rigorous fracture assessment becomes critical to ensure the safety and serviceability of the infrastructures [2], [5]. Furthermore, the microstructure of concrete comprising of aggregate, paste and ITZ (Interfacial Transitional Zone) in macro-scale plays a substantial role in defining the crack propagation and overall fracture behavior of concrete.

In this regard, there has been significant attention on improving the microstructure, focusing on alternative binders and/or aggregate to improve the fracture behavior [6], [7], [8]. A significant aspect of these studies is related to enhance the packing of overall microstructure. This enhanced packing is also aligned with the objective of attaining low carbon concrete as an improvement of packing also lowers the cement content of the mixes [9], [10], [11]. As coarse aggregates occupy 70% of a concrete matrix, and provide durability, strength, toughness, skid resistance, and dimensional stability, it is vital to understand the role of aggregate packing on the fracture behavior. Previous studies have also studied the role of aggregate morphology on packing and relevant concrete properties [6]. To the best of the authors' knowledge, there are limited studies focusing on the effect of particle packing of the aggregate skeleton in fracture response of concrete.

Conventional fracture assessment studies mostly focus on the overall load – Crack Mouth

Opening Displacement (CMOD) or load-displacement curve. However, the crack propagation and the subsequent strain jump mostly occurs in the vicinity of the 95% pre and post peak regime [12], [13]. Hence, it is crucial to segregate the fracture response within this "nearby peak regime", in addition to the overall load-CMOD response, to ensure a comprehensive understanding of the fracture behavior. The rapid progression of cracks and an accurate measurement of crack characteristics necessitates the use of high-speed imaging [14].

This study focuses on identifying the role of packing of aggregate skeleton on the overall fracture properties of 4 unique concrete mixes (M1-M4). The mixes here have been optimized by changing the packing of the coarse aggregate, comprising the major portion of the concrete volume. Here, we show the role of packing efficiency on the overall fracture properties of the concrete specimen. To track the fracture properties at the 95% pre and post peak regime, we employ a high-speed camera that effectively captures fracture behavior of cross-sectional concrete samples. Using the Load-CMOD curve and the Two-Parameter Fracture Model (TPFM), the effect of aggregate packing on compressive strength, peak flexural load, fracture energy, and critical stress intensity factor has been evaluated.

Specifically, we quantify the role of packing efficiency on the overall fracture properties of the concrete specimens. Here, we show that increasing the packing efficiency from 88% (M1) to 93% (M4) resulted in an increase in 3 and 7-day compressive strength by 15.29% (36.7 MPa to 42.31 MPa) and 11.13% (43.62 MPa to 48.47 MPa). Meanwhile, for fracture energy (G_f) obtained using Hillerborg's work of fracture [15], [16], a similar increase in packing efficiency, enhanced G_f by 35.29% (79.96 N/m for M1 to 108.18 N/m for M4) and 39.48% (130.05 N/m for M1 to 181.40 N/m) for 3 and 7 days of hydration respectively. Similarly, for critical stress intensity factor (K_{1C}) obtained by employing high-speed digital image correlation and TPFM, a significant increase of 46.08% and 51.66% was observed for M4 (1.03 MPa$\sqrt{m}$ and 1.30 MPa$\sqrt{m}$) compared to M1 (0.71 MPa$\sqrt{m}$ and 0.86 MPa$\sqrt{m}$) at 3 and 7 days of hydration. Overall, this study highlights the significance of aggregate packing optimization to enhance the fracture response of concrete- without altering the binder composition. By harnessing this approach, it becomes possible to design and formulate eco-efficient concrete mixes that can pave the way for more sustainable and resilient infrastructures.

2 METHODS & MATERIALS

2.1 Materials used

Here, Type IL cement (Portland Limestone Cement or PLC) with low alkali content was used as the cementitious material. The elemental composition of CaO, SiO_2, Al_2O_3 and Fe_2O_3 were 62.9%, 20.6%, 4.4% and 3.3%, respectively. The Specific Gravity (SG) of the cement used was 3.06 and Blaine's fineness was 479 m^2/kg. Natural sand from the lab with a SG of 2.62, Absorption Capacity (AC) of 1.87% and Moisture Content (MC) of -1.65% was used as the fine aggregate. The particle size distribution (PSD) of both the PLC and fine aggregate is shown in **Figure 1**. The PSD of the fine aggregate in the matrix were measured in accordance with ASTM C136.

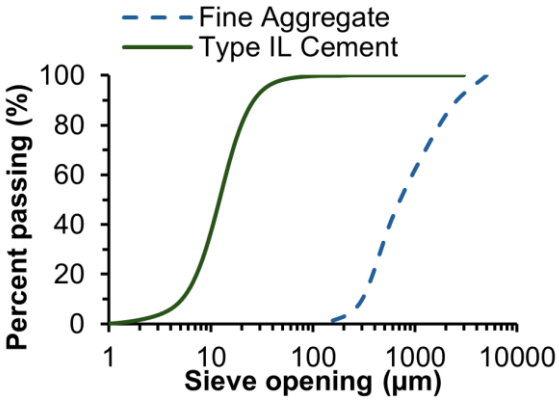

Figure 1. Particle Size Distribution of fine aggregates of the lab measured in accordance with ASTM C136 and Particle Size Distribution of Type IL cement used in the study and obtained from the manufacturer.

Natural limestone aggregates from the lab stockpile with a Nominal Maximum Aggregate Size (NMAS) of 9.5 mm were used to

investigate the influence of coarse aggregates in the fracture response of concrete. The AC and the MC of the coarse aggregates were 4.62% and -2.6% respectively. The aggregates were used from stockpile in the lab and the moisture content calculated was accounted for during the mix design for both coarse and fine aggregates. Thus, a constant mass-based water-cement ratio $(w/c)_m$ of 0.45 was maintained for all the mixes. Furthermore, a coarse aggregate-to-binder ratio of about 1.65 was used to prioritize the role of packing optimization of the coarse aggregate in these systems. The proportion of the concrete mixture used in this study is presented in **Table 1.**

Table 1. Mix proportioning of the concrete mixture used in the study. Constant proportions were utilized for duration of the study with a varying packing morphology of the coarse aggregate only.

Component	Proportion used (kg/m^3)
Cement	555
Water	250
Fine Aggregate	600
Coarse Aggregate	910
Total	**2315**

2.2 Mix design and sample preparation procedure

The mixtures used had different packing morphologies obtained by proportioning coarse aggregates through five different sieves (19 mm, 16 mm, 12 mm, 9.5 mm, and 4.75 mm). The proportions of coarse aggregates retained in each sieve for the four mixes are given in **Table 2**. The nomenclature of the mixes is based on an ascending packing efficiency of the coarse aggregates (CA1 < CA2 < CA3 < CA4). The packing morphologies of the coarse aggregate obtained is shown in **Figure 2**. A detailed procedure to assess the packing efficiency is given in **Section 2.3**. The concrete mixtures obtained from this process are named M1, M2, M3, and M4, based on the difference in packing efficiency, and obtained by varying the packing morphologies of the coarse aggregate in the mixes.

Table 2. Percentage Fraction of Coarse Aggregate added in each mix based on the aggregate retained in the respective sieve size.

Proportion of the Coarse Aggregate (%)				
Sieve Size (mm)	**M1**	**M2**	**M3**	**M4**
19	100	60.4	30.8	11
16	0	22	23.6	11
12	0	11	13.7	18.1
9.5	0	3.3	22	40.1
4.75	0	3.3	9.9	19.8
Packing efficiency (%)	88	90	92	93

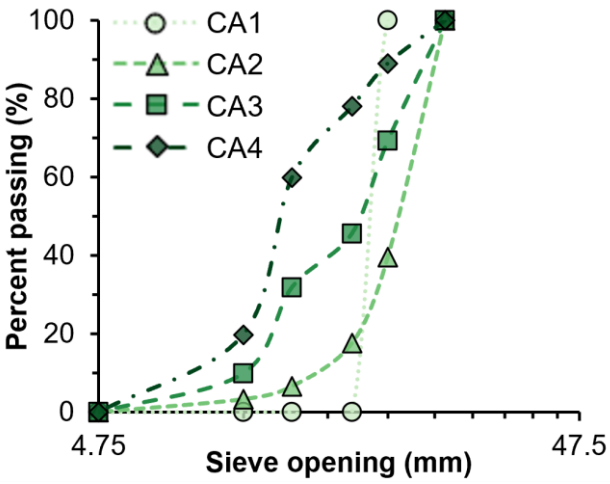

Figure 2. Modified particle size profiling of the coarse aggregate for packing optimization. The gradation details along with the specific proportions of coarse aggregates used in each mix are mentioned in Table 2.

Finally, prismatic samples (200 mm × 50 mm × 50 mm) were employed for flexural/fracture testing and cylinders (100 mm × 200 mm) were employed for compressive strength assessment. The specimens were cured in an ambient temperature of 23 ± 2 ^{0}C and 95% relative humidity until the desired testing age of 3 and 7 days.

2.3 Experimental techniques

2.3.1 Packing optimization

In this study, the Modified Anderson and Andreasen (MAA) Model [17] has been used to compare the ideal packing condition, as represented in **Eq. (1)**.

$$P(D) = \left(\frac{D^q - D_{min}^q}{D_{max}^q - D_{min}^q}\right)^q \times 100\% \quad (1)$$

where,

P(D) is the fraction of particles finer than diameter "D",

and D_{min} and D_{max} are the minimum and maximum particle size used in the system.

The distribution modulus, q, is a key parameter that influences the particle size distribution curve and determines the balance between the coarse and fine particles [6]. Lower q represents a finer mix whereas a higher q represents a mix with more coarse particles. In this case, a q value of 0.37 was adopted to account for the addition of both coarse and fine particles, which is closer to what has been used in previous studies [8], [18].

The packing profile of the mixes were evaluated, in terms of the packing efficiency, based on the difference between MAA and the composite size profile of the mixes which is further illustrated in **Figure 3**. The packing efficiency of all four mixes M1-M4 were calculated from Eq. (2).

$$Packing\ Efficiency = \left(1 - \sqrt{\sum_{i=1}^{n}\left(P_M(D_i^{i+1}) - P_0(D_i^{i+1})\right)^2}\right) \times 100\% \quad (2)$$

where,

P_M is the % passing obtained for No. i^{th} sieve for a specific mix.

and P_0 is the % passing obtained for the same i^{th} sieve in the ideal MAA curve.

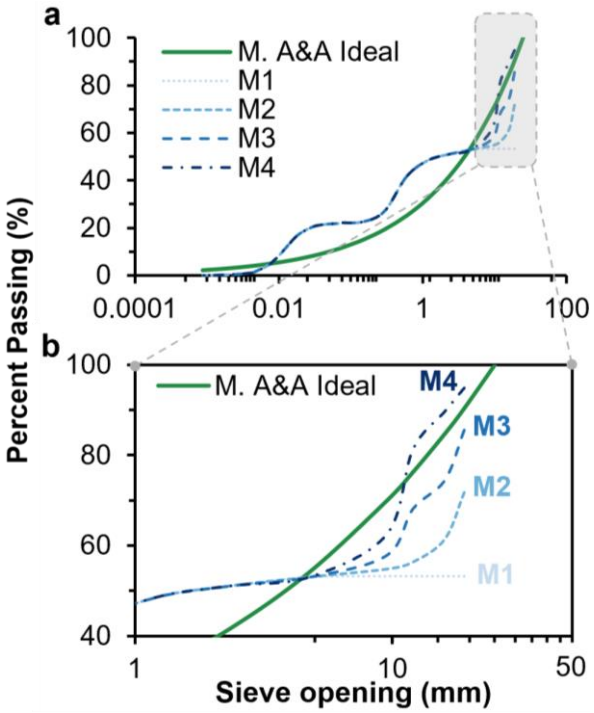

Figure 3. (a) Composite size profile of mixes M1-M4 obtained from PSD of constituents. The ideal packing condition is represented by the green line, as obtained from the MAA model. (b) Portion of the overall size profile contributed by the variation in coarse aggregate packing.

2.3.2 Cross sectional exposure and notch addition

Firstly, slabs of size 200 mm × 100 mm × 50 mm were cast. A diamond edge concrete saw was utilized to slice the specimen in half to expose the aggregate skeleton of the matrix along plane A-A as shown in **Figure 4 (a)** and **(b)**. The same saw was used to add a notch in the prisms along plane B-B as shown in **Figure 4 (a)**. The notch-depth to beam-depth ratio (a_o/D) was 0.25 (a_o = 12.5 mm) as depicted in **Figure 4 (c)**. The notch was placed downwards during the test and a clip gauge was mounted with the help of a knife edge to measure the crack mouth opening displacement (CMOD) in the beams during the test.

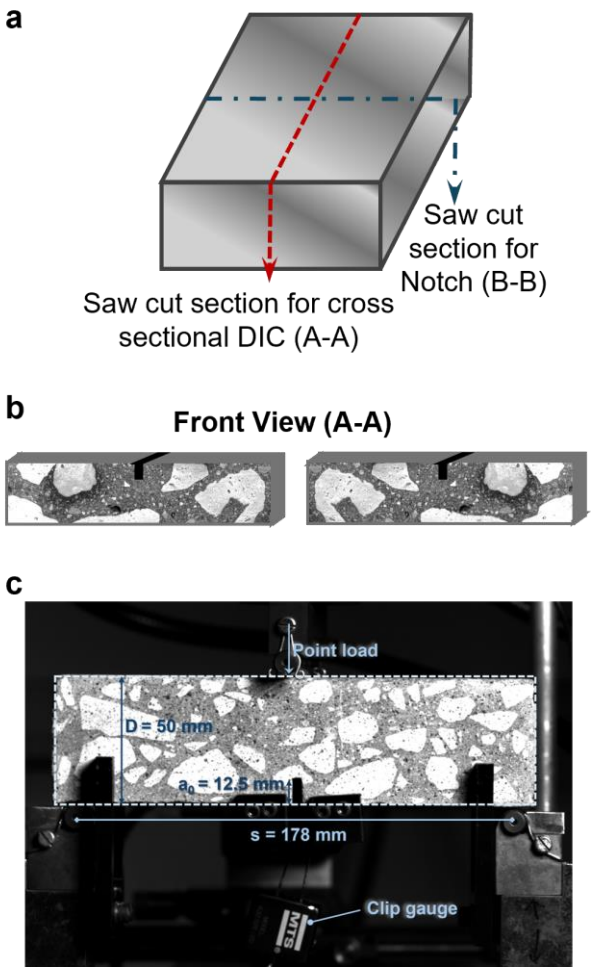

Figure 4. (a) Slabs cast to obtain beam samples for fracture testing. A diamond edge concrete saw was used in the longitudinal direction to expose the aggregates and obtain a cross sectional DIC. The same saw was used to add a notch to the transverse direction of the beams. (b) Front view for section A-A illustrating the beams obtained after the slicing of the slabs in both transverse and longitudinal direction. (c) Experimental setup for the three-point bending test (3PBT) on notched beam samples. A CMOD-controlled test of 0.1 mm/min was carried out during both the loading and unloading cycles in the MTS machine. A clip gauge was mounted on the notch with the help of a knife edge to measure the CMOD obtained during the test.

2.3.3 Compressive strength

The effect of aggregate packing optimization on the mechanical performance of the matrix was determined by testing 100 mm × 200 mm cylindrical specimens. Before testing, the cylinders were capped using Neoprene rubbers to ensure a flat surface and reduce variance in the strength results. The compressive strength was determined confirming to ASTM C39 at 3 and 7 days of curing using a Forney compressive testing machine with a constant loading rate of 27,000 ± 5,000 lb./min.

2.3.4 Determination of flexural strength and fracture properties

The flexural strength was measured using standard three-point bending (3PBT) confirming to ASTM C293/C293M – 16. Sliced rectangular beams of size 200 mm (length, l) × 50 mm (width, t) × 50 mm (depth, D) and span (s) of about 178 mm (7”) were used.

The Two-Parameter Fracture Model (TPFM) was used to characterize the fracture property of three replicate beams for all four mixes [2], [16]. Crack Mouth Opening Displacement (CMOD) controlled mode of 0.1 mm/min was utilized during both loading and unloading cycles. CMOD was measured using a clip gauge placed under the notch using a knife edge of 1.5 mm thickness. The knife edge was glued onto a 3D printed mold which exactly fit over the width of the beam. Various fracture parameters like critical stress intensity factor (K_{1C}), fracture energy (G_f) along with peak load and CMOD were assessed from the load-CMOD conducted test using a servo-hydraulic load frame.

The fracture energy (G_f) for mixes M1-M4 were determined at 3 and 7 days of hydration using Hillerborg’s work of fracture method as shown in Eq. (3) [15], [16].

$$G_f = \frac{W_0 + 2P_w\delta_0}{(D - a_0)t} \qquad (3)$$

where, W_0 is the area under the Load-CMOD curve,

P_w is the self-weight of the beam

and δ_0 is the CMOD at failure.

The loading-unloading cycles were conducted to determine compliance, which can be utilized to calculate the stress energy release rate (G_R).

The stress intensity factor – K_{1C} in failure mode I (opening), which expresses the strength of the singular elastic stress field was calculated using **Eq. (4)** of the TPFM [2] [19]. TPFM is useful to determine both K_{1C} and critical crack tip opening displacement ($CTOD_c$), however, only K_{1C} is covered in this study.

$$K_{1C} = \frac{3P_{max}s}{2BW^2}\sqrt{\pi a_{eff}}\,F(\alpha) \qquad (4)$$

where,

a_{eff} is the effective crack length.

$$a_{e_{ff}} = a_0 + \Delta a \qquad (5)$$

and Δa is the crack extension length, which was obtained from the non-contact DIC method by utilizing time stamps at specific load regimes.

$$F(\alpha) = \frac{1}{\sqrt{\pi}}\frac{1.99-\alpha\,(1-\alpha)(2.15-3.95\alpha+2.7\alpha^2)}{(1+2\alpha)(1-\alpha)^{\frac{3}{2}}} \qquad (6)$$

where,

α = a/W, P_{max} is the maximum load.

2.3.5 High-speed Cross-sectional Digital Image Correlation (DIC)

The crack path tortuosity, crack geometry, crack extension length, and crack tip opening displacement (CTOD) was determined using a non-contact speckle tracking in the beams. A high-speed camera was used to record images at 2000 frames per second (fps) prior to load drop. After the images were captured, an analysis region close to the notch was selected to perform the DIC analysis using VIC-2D software™ provided by Correlated Solutions [20, p. 2]. The step size and subset were chosen to accommodate the displacement of each speckle pattern. The speckle patterns were obtained by spraying black and white paints over the cross section of the beam. Exposing the aggregate skeleton provided improved understanding on the crack propagation path and Fracture Process Zone (FPZ).

3 RESULTS AND DISCUSSION

3.1 Early age compressive strength

The effect of packing efficiency, as summarized in **Table 2**, on the early-age strength of the concrete mixes is shown in **Figure 5**. The strength assessment has been conducted for 3- and 7-days of curing, since the effect of packing is usually more evident at an earlier age of hydration [6]. **Figure 5** shows that the early-age strength of the concrete specimens increased significantly with an increase in packing efficiency. Evidently, mix M4 with the highest packing efficiency of 93% exhibited a 15.29% increase in 3-day compressive strength, as compared to mix M1 (36.72 MPa for M1 to 42.31 MPa for M4) with the lowest packing efficiency of 88%. A similar trend has been observed at 7-days of hydration with mix M4 exhibiting 11.13% increase in strength compared to mix M1 (43.62 MPa for M1 to 48.47 MPa for M4). The increase in strength with improved packing efficiency can be attributed to an improved load-transfer phenomenon in a well-packed system. Improved packing efficiency signifies a higher number of contact points in between the aggregates per unit volume, which leads to an increase in the point of contacts for efficient load transfer and increases the strength [6].

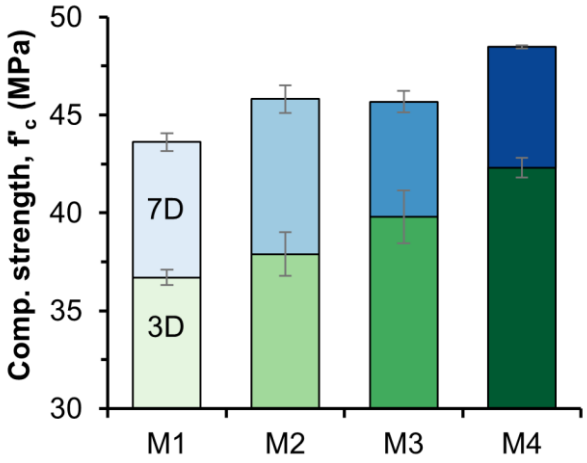

Figure 5. Effect of particle packing on early age compressive strength development of mixes M1 – M4. The error bars represent the standard deviation from 3 samples of each mix. The blue shade in the graph refers to strength obtained for mixes M1-M4 at 3 days of hydration and the green shade refers to the strength obtained at 7 days of hydration.

3.2 Fracture response and fracture energy of the mixes

The fracture responses have been evaluated from load-crack mouth opening displacement (CMOD) plot. Load-CMOD response for all the mixes at 3 days of hydration is represented in **Figure 6**. Mix M4, with the highest packing efficiency has a peak load 35.69% (1.55kN for M4) greater than mix M1 (1.15 kN for M1) with the lowest packing efficiency. A similar trend was observed at 7 days of hydration with M4

(2.06 kN) exhibiting 44.06% higher flexural load than M1 (1.43 kN). **Figure 7** shows that the peak flexural load obtained for each mix at 3 and 7 days of hydration improved with an increase in the packing efficiency.

From the load-CMOD test and **Eq. (3)**, fracture energy (G_f) of the mixes were calculated at 3 and 7 days of hydration which is shown in **Figure 8**. With an increase in packing efficiency, G_f for M4 (108.18 N/m and 181.40 N/m) was 35.29% and 39.48% higher than for M1 (79.96 N/m and 130.05 N/m) at 3 and 7 days of hydration, respectively. In addition to the effective load transfer, an improved bonding surface area and dense microstructure with reduced porosity can be expected in a mix with higher packing efficiency [21], [22], [23]. Thus, there is a delay in onset of cracking and enhancement in crack resistance of the mixes which increases both the peak flexural load and the fracture energy of the matrix.

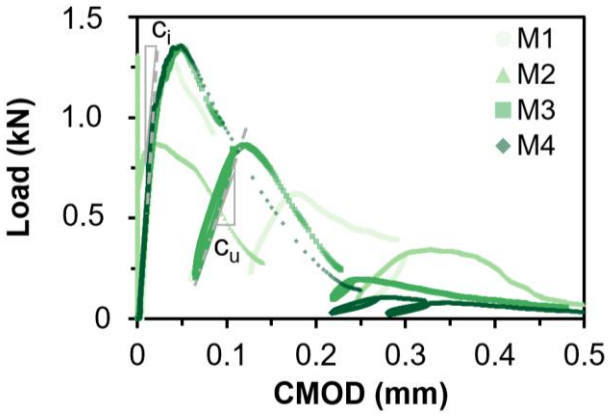

Figure 6. Representative Load-CMOD plot for mixes M1-M4 at 3 days of hydration. c_i and c_u represent loading and unloading compliances respectively for M3 which is used to determine the parameters required for TPFM from the plot.

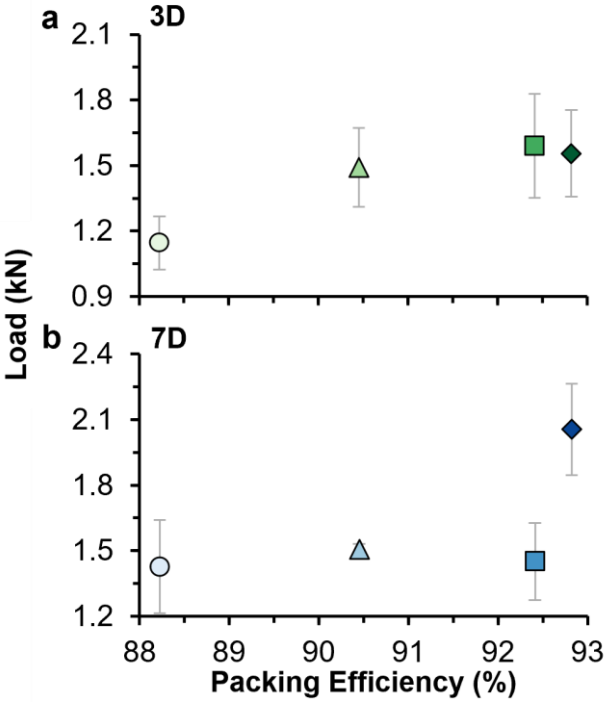

Figure 7. Effect of packing efficiency on the maximum load sustained by mixes M1-M4 at (a) 3 days and (b) 7 days of hydration, obtained from the 3PBT test. The error bars represent the standard deviation in maximum load obtained for three different specimens of each mix.

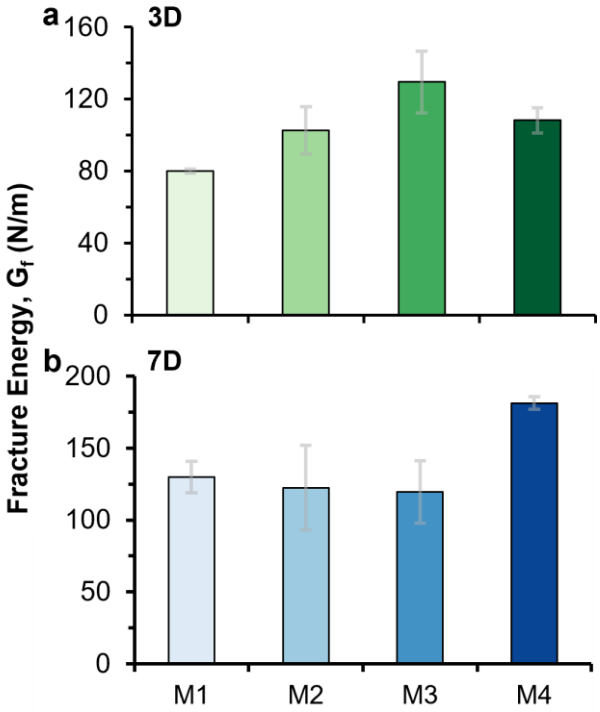

Figure 8. Effect of packing efficiency on the fracture energy of the mixes M1-M4 at (a) 3 days and (b) 7 days of hydration. The fracture energy represents the area under the load-CMOD curve. The error bars represent

the standard deviation of the fracture energy obtained from 3 samples of each mix.

3.3 Fracture toughness of the mixes

The efficacy of increasing packing efficiency in enhancing the values of stress intensity factor (K_{1C}) is shown in **Figure 9**. A significant increase of 46.08% and 51.66% in K_{1C} was observed for M4 (1.03 MPa$\sqrt{m}$ and 1.30 MPa$\sqrt{m}$) compared to M1 (0.71 MPa$\sqrt{m}$ and 0.86 MPa$\sqrt{m}$) at 3 and 7 days of hydration, respectively. Following on the previous concept of an improved microstructure of the concrete with an increase in packing efficiency, the crack path obtained for M4 (packing efficiency 93%) will be more tortuous and complex compared to M1 (packing efficiency 88%) [21], [24]. The concept of an increased crack path is visually illustrated in **Figure 10**. Due to an increase in the packing efficiency or enhancement in packing optimization, there is a higher degree of aggregate interlocking which is also responsible for increasing the crack extension length and the fracture toughness of the mix [22], [24], [25]. **Figure 10** shows that the crack extension length for M4 is much more branched and tortuous compared to M1 which is primarily due to the increased packing efficiency.

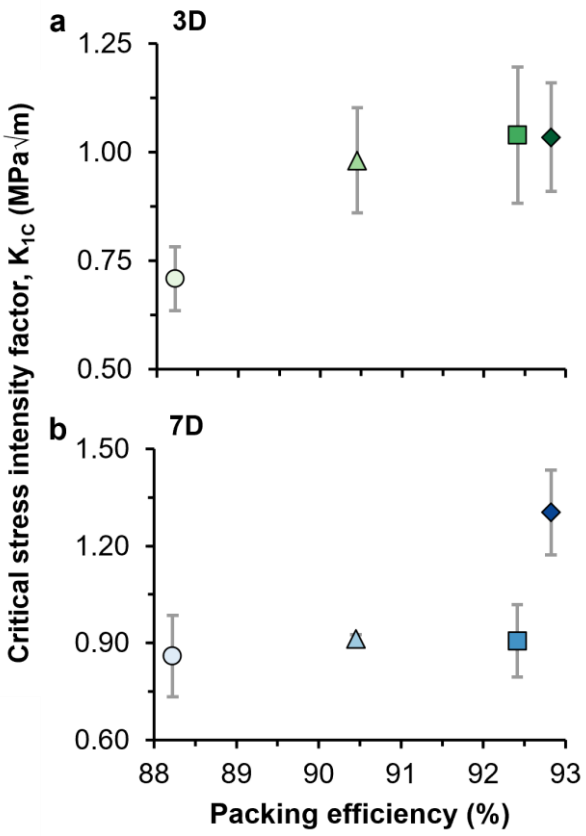

Figure 9. Effect of packing efficiency on the critical stress intensity factor of the mixes M1-M4 at (a) 3 days and (b) 7 days of hydration. The critical stress intensity factor is calculated from DIC results and TPFM. Error bars in the plot represent the standard deviation obtained from three representative samples of each mix.

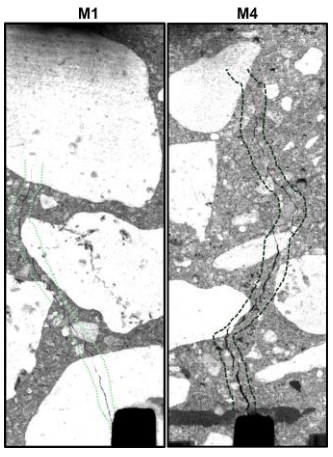

Figure 10. Representative crack extension length obtained for M1 and M4 at 3 days of hydration from high-speed DIC at micro-segmented peak load regime. After the micro-segmentation of the peak load, the crack extension length could be monitored at specific intervals within the propagation period that helped understand the strain development during 95% pre-peak to peak load regime.

4 CONCLUSIONS

Sustainability in concrete can be achieved by optimizing particle packing of the mix components. While considerable work has been performed to enhance packing efficiency, its impact on the fracture properties of concrete remains underexplored. Given the quasi-brittle nature of concrete, fracture behavior is critical to understand the failure mechanism. This study investigated the influence of aggregate packing efficiency on the mechanical and fracture response of four concrete mixes after 3 and 7 days of curing periods.

Three major conclusions were attained from this study. Firstly, improved packing efficiency significantly enhanced compressive strength. For a packing efficiency of 93% (M4), compressive strength increased by 15.29% and 11.13% at 3 and 7 days, respectively, compared to a packing efficiency of 88% (M1). This improvement underscores the role of a well-packed matrix in enhancing the strength.

Secondly, analysis of Load - crack mouth opening displacement (CMOD) curves and Hillerborg's work of fracture showed substantial increment in fracture energy and peak load for M4. At 3 days, increases of 35.69% and 35.29% were observed, while at 7 days, fracture energy and peak flexural load rose by 39.48% and 44.06%, respectively, compared to M1.

Finally, critical stress intensity factor (K_{1C}) values obtained through the two-parameter fracture model (TPFM) demonstrated improvements of 46.08% and 51.66% at 3 and 7 days, respectively, for M4 compared to M1, emphasizing the impact of aggregate packing on fracture resistance.

In summary, optimizing aggregate packing efficiency enhances both fracture and mechanical properties, paving the way for eco-efficient and resilient concrete. This approach aligns with the concrete industry's goal of achieving sustainability without altering binder content.

REFERENCES

[1] Z. P. Bažant, "Fracture in Concrete and Reinforced Concrete," John Wiley & Sons, 1985.

[2] "Two Parameter Fracture Model for Concrete." Accessed: Dec. 02, 2024. [Online]. Available: https://ascelibrary.org/doi/epdf/10.1061/%28ASCE%290733-9399%281985%29111%3A10%281227%29

[3] Ł. Skarżyński, M. Nitka, and J. Tejchman, "Modelling of concrete fracture at aggregate level using FEM and DEM based on X-ray μCT images of internal structure," *Engineering Fracture Mechanics*, vol. 147, pp. 13–35, Oct. 2015, doi: 10.1016/j.engfracmech.2015.08.010.

[4] W. Trawiński, J. Bobiński, and J. Tejchman, "Two-dimensional simulations of concrete fracture at aggregate level with cohesive elements based on X-ray μCT images," *Engineering Fracture Mechanics*, vol. 168, pp. 204–226, Dec. 2016, doi: 10.1016/j.engfracmech.2016.09.012.

[5] J. Mazars, "A description of micro- and macroscale damage of concrete structures," *Engineering Fracture Mechanics*, vol. 25, no. 5, pp. 729–737, Jan. 1986, doi: 10.1016/0013-7944(86)90036-6.

[6] B. Baten and N. Garg, "Introducing Particle Shape Metric (PSM): A fundamental parameter that encapsulates role of aggregate shape in enhancing packing and performance," *Cement and Concrete Research*, vol. 182, p. 107558, Aug. 2024, doi: 10.1016/j.cemconres.2024.107558.

[7] R. Yu, P. Spiesz, and H. J. H. Brouwers, "Development of an eco-friendly Ultra-High Performance Concrete (UHPC) with efficient cement and mineral admixtures uses," *Cement and Concrete Composites*, vol. 55, pp. 383–394, Jan. 2015, doi: 10.1016/j.cemconcomp.2014.09.024.

[8] K. A. Ragalwar, H. Nguyen, R. Ranade, W. F. Heard, and B. A. Williams, "Influence of Distribution Modulus of Particle Size Distribution on Rheological and Mechanical Properties of Ultra-High-Strength SHCC Matrix," in *Strain-Hardening Cement-Based Composites*, V. Mechtcherine, V. Slowik, and P. Kabele, Eds., Dordrecht: Springer Netherlands, 2018, pp. 221–229. doi: 10.1007/978-94-024-1194-2_26.

[9] B. Baten, M. J. Gombeda, N. Garg, Illinois Center for Transportation, and University of Illinois at Urbana-Champaign. Department of Civil and Environmental Engineering, "Utilizing a Particle-Packing Approach for an Illinois-Specific, Nonproprietary, Low-Shrinkage UHPC," FHWA-ICT-24-018, Sep. 2024. doi: 10.36501/0197-9191/24-021.

[10] K. L. Scrivener, V. M. John, and E. M. Gartner, "Eco-efficient cements: Potential economically viable solutions for a low-CO2 cement-based materials industry," *Cement and Concrete Research*, vol. 114, pp. 2–26, Dec. 2018, doi: 10.1016/j.cemconres.2018.03.015.

[11] A. Witte and N. Garg, "Quantifying the global warming potential of low carbon concrete mixes: Comparison of existing life cycle analysis tools," *Case Studies in Construction Materials*, vol. 20, p. e02832, Jul. 2024, doi: 10.1016/j.cscm.2023.e02832.

[12] S. Das *et al.*, "The fracture response of blended formulations containing limestone powder: Evaluations using two-parameter fracture model and digital image correlation," *Cement and Concrete Composites*, vol. 53, pp. 316–326, Oct. 2014, doi: 10.1016/j.cemconcomp.2014.07.018.

[13] S. Das, M. Aguayo, G. Sant, B. Mobasher, and N. Neithalath, "Fracture process zone and tensile behavior of blended binders containing limestone powder," *Cement and Concrete Research*, vol. 73, pp. 51–62, Jul. 2015, doi: 10.1016/j.cemconres.2015.03.002.

[14] X. Zhang, S. Li, Y. Qin, J. Chai, Z. Xu, and Z. Si, "New Method for Investigating Crack Development in Concrete Using an Ultrahigh-Speed Camera," *Journal of Materials in Civil Engineering*, vol. 31, no. 1, p. 04018357, Jan. 2019, doi: 10.1061/(ASCE)MT.1943-5533.0002578.

[15] A. Hillerborg, "The theoretical basis of a method to determine the fracture energyGFof concrete," *Materials and Structures*, vol. 18, no. 4, pp. 291–296, Jul. 1985, doi: 10.1007/BF02472919.

[16] J. Roesler, G. H. Paulino, K. Park, and C. Gaedicke, "Concrete fracture prediction using bilinear softening," *Cement and Concrete Composites*, vol. 29, no. 4, pp. 300–312, Apr. 2007, doi: 10.1016/j.cemconcomp.2006.12.002.

[17] J. E. Funk and D. R. Dinger, *Predictive Process Control of Crowded Particulate Suspensions*. Boston, MA: Springer US, 1994. doi: 10.1007/978-1-4615-3118-0.

[18] H. Karimi and H. J. H. Brouwers, "A Particle Packing Method for Pumpable Low-Shrinkage Flowing Concrete", Accessed: Dec. 07, 2024. [Online]. Available: https://www.concrete.org/publications/internationalconcreteabstractsportal.aspx?m=details&id=51738685

[19] L. C. S. Nunes and J. M. L. Reis, "Estimation of crack-tip-opening displacement and crack extension of glass fiber reinforced polymer mortars using digital image correlation method," *Materials & Design*, vol. 33, pp. 248–253, Jan. 2012, doi: 10.1016/j.matdes.2011.07.051.

[20] "VIC-2D Digital Image Correlation," Correlated Solutions Digital Image Correlation. Accessed: Dec. 09, 2024. [Online]. Available: https://www.correlatedsolutions.com/vic-2d

[21] S. Khalilpour, E. BaniAsad, and M. Dehestani, "A review on concrete fracture energy and effective parameters," *Cement and Concrete Research*, vol. 120, pp. 294–321, Jun. 2019, doi: 10.1016/j.cemconres.2019.03.013.

[22] A. P. N. Siregar, M. I. Rafiq, and M. Mulheron, “Experimental investigation of the effects of aggregate size distribution on the fracture behaviour of high strength concrete,” *Construction and Building Materials*, vol. 150, pp. 252–259, Sep. 2017, doi: 10.1016/j.conbuildmat.2017.05.142.

[23] P. C. Strange and A. H. Bryant, “The role of aggregate in the fracture of concrete,” *J Mater Sci*, vol. 14, no. 8, pp. 1863–1868, Aug. 1979, doi: 10.1007/BF00551025.

[24] B. Chen and J. Liu, “Effect of aggregate on the fracture behavior of high strength concrete,” *Construction and Building Materials*, vol. 18, no. 8, pp. 585–590, Oct. 2004, doi: 10.1016/j.conbuildmat.2004.04.013.

[25] P. Goltermann, V. Johansen, and L. Palbøl, “Packing of Aggregates: An Alternative Tool to Determine the Optimal Aggregate Mix”, Accessed: Dec. 09, 2024. [Online]. Available: https://www.concrete.org/publications/internationalconcreteabstractsportal/m/details/id/328